Available online at www.sciencedirect.com
SCIENCE DIRECT
Thin Solid Films 510 (2006) 275 – 279
thin solid films
www.elsevier.com/locate/tsf

$YNi_xMn_{1-x}O_3$ thin films by pulsed laser deposition: Structure and magnetic properties

Yanwei Ma [a,b,*], M. Guilloux-Viry [b], P. Barahona [b], O. Peña [b], C. Moure [c], J. Ghilane [d], P. Hapiot [d]

[a] Applied Superconductivity Lab., Institute of Electrical Engineering, Chinese Academy of Sciences, P.O. Box 2703, Beijing 100080, China
[b] Chimie du Solide et Inorganique Moléculaire, UMR 6511, CNRS–Université de Rennes 1–Institut de Chimie de Rennes, 35042 Rennes Cedex, France
[c] Instituto de Ceramica y Vidrio, CSIC, campus de Cantoblanco, 28049 Madrid, Spain
[d] Laboratoire d'Electrochimie Moléculaire et Macromoléculaire, SESO, UMR 6510 CNRS—Université de Rennes 1, 35042 Rennes, France

Received 6 June 2005; received in revised form 2 November 2005; accepted 7 December 2005
Available online 7 February 2006

Abstract

Highly oriented $YNi_xMn_{1-x}O_3$ thin films on $SrTiO_3$ (100) substrates were achieved by using pulsed laser deposition for $x=0.33$ and $x=0.50$. We used a combination of X-ray diffraction, scanning electron microscopy, atomic force microscopy, and magnetic-property measurements. The magnetic transition temperatures (T_c) of the as-grown films are higher than the corresponding bulk values (typically 85 K instead of 80 K, for $x=0.5$, and 60 K instead of 50 K, for $x=0.33$). Our magnetic measurements also suggest a spin-glass characteristic in the $x=0.33$ films, while a cluster glasslike behavior is observed for the films with $x=0.5$, which is quite different from that of the bulk samples. Finally, the influence of post-deposition heat treatment on the magnetic properties of the as-grown films is discussed.

Keywords: Pulsed laser deposition; Magnetic properties; Surface morphology; Doped manganite

1. Introduction

Doped perovskite manganites $REMnO_3$ (RE=rare-earth elements) have been extensively studied over the last decade. This system is found to exhibit fascinating properties [1,2], such as metal–insulator transition, ferromagnetic (FM) – paramagnetic (PM) phase transition, colossal magnetoresistance, charge and orbital ordering, etc., which can be very useful for the development of new magnetic and magnetoresistive devices. In general, the magnetic properties of the manganites were explained by the double-exchange (DE) mechanism [3] combining with the local Jahn–Teller distortions of Mn^{3+} ions [4].

On the other hand, there are only a few reports on doping the Mn-site of the $REMnO_3$ perovskite, in which manganese can be partially substituted by divalent transition elements (e.g., Cu^{2+}, Co^{2+}, Ni^{2+}...). It can be expected that elements of lower valence than Mn^{3+} could also induce the formation of Mn^{4+} cations, when incorporated in the solid solution. Recently, concerning this type of substitution in the $YNi_xMn_{1-x}O_3$ bulk system, we have reported a phase transition from hexagonal $YMnO_3$ type structure to orthorhombic structure for Ni substitution above 20 at.%, along with a semi-conducting behavior of the perovskite phase [5]. Besides that, the magnetic regime was found to depend on the relative concentration of the substituent, changing from antiferromagnetism ($x<0.33$) to ferromagnetism ($x>0.33$) [6].

In order to integrate these functional materials into technological devices, it is of first importance, in a first step, to study their behavior in the form of thin films, since films can exhibit different properties compared to their bulk counterpart. In this respect, we have undertaken the elaboration of thin films of $YNi_xMn_{1-x}O_3$, for some x(Ni) compositions ($x=0.33$ and 0.5). These two particular compositions were chosen because the magnetic behavior for $x=0.33$ bulk is spin canted-like, whereas it is fully ferromagnetic for $x=0.5$. In this paper, we report on the structural and magnetic properties of $YNi_xMn_{1-x}O_3$ thin films epitaxially grown on $SrTiO_3$ (100) substrates.

* Corresponding author.
E-mail address: ywma@mail.iee.ac.cn (Y. Ma).

0040-6090/$ - see front matter © 2005 Elsevier B.V. All rights reserved.
doi:10.1016/j.tsf.2005.12.159

2. Experimental details

Thin films of $YNi_xMn_{1-x}O_3$ (YNMO) were grown using pulsed laser deposition. Deposition was performed from targets with stoichiometric composition of $YNi_xMn_{1-x}O_3$ ($x=0.33$, 0.5). Films were synthesized on $SrTiO_3$ (100) substrates (cubic, $a=3.905$ Å). A detailed description of the deposition system is mentioned elsewhere [7]. In brief, a 248 nm KrF pulsed laser with 2 Hz repetition rate and 2 J/cm^2 energy density was used. Deposition was performed at 740 °C under an oxygen pressure of 25–60 Pa. Following the deposition, the films were cooled down to room temperature (T) at a rate of about 35 °C/min in 26656 Pa of oxygen. All films had a thickness around 200 nm. Some samples were subjected to post-deposition annealing in oxygen at 850 °C for 10 h.

X-ray diffraction (XRD) with a high-resolution four-circle texture diffractometer (Brüker AXS D8 Discover) and $CuK_{\alpha 1}$ radiation ($\lambda=1.54056$ Å). The films' microstructure was observed using a field effect scanning electron microscopy (SEM) by the operating voltage of 7 kV. Field-cooled (FC) and zero-field-cooled (ZFC) magnetization was measured at various applied fields in a superconducting quantum interference device magnetometer. The applied fields (H) were in the film plane. The magnetization measurement was performed for several film samples to check reproducibility.

3. Results and discussion

Fig. 1 displays the $\theta-2\theta$ X-ray diffraction patterns of the YNMO films ($x=0.33$ and 0.5). Only 00l diffraction peaks of the phase are present evidencing a highly oriented film with the c-axis perpendicular to the surface of the substrate. We did not see any trace of impurities, at least at the scale of the XRD detection. The estimated value of the out-of-plane lattice parameter for the films with $x=0.33$ was $c/2=3.745$ Å, and $c/2=3.746$ Å for $x=0.5$, which are slightly higher than the corresponding bulk values (3.725, 3.706 Å, respectively). Note that the structure of the bulk YNMO was found to be orthorhombic (*Pbnm*). For $x=0.5$, the lattice constants are $a/\sqrt{2}=3.692$ Å, $b/\sqrt{2}=4.007$ Å, $c/2=3.706$ Å. As expected for epitaxial films, the in-plane lattice parameters a and b match the substrate of $SrTiO_3$ (cubic, $a=3.905$ Å) provided that the film crystal lattice is rotated by 45° with respect to the substrate. As usually observed when the film crystallizes in an orthorhombic system whereas the substrate crystallizes in a cubic one, then the epitaxial relations are: $(00l)_{film}$ // $(00l)_{SrTiO3}$, $[100]_{film}$ // $[011]_{SrTiO3}$. Therefore, the YNMO/STO films have the film–substrate lattice mismatch ~5.4% along the a direction and ~−2.6% along the b direction, with their in-plane lattice parameters expanded and compressed, respectively. This clearly indicates the large lattice mismatch between YNMO and STO.

In order to investigate the structural quality of these YNMO films, the rocking curves of the 004 peaks were carried out (ω-scans). The full width at half maximum (FWHM) of both films is around 1°. Furthermore, the four peaks at 90° intervals in the φ-scan of the $x=0.33$ film (see inset of Fig. 1b) are the signature of an in-plane order of the film. Similar diffraction profile were obtained in the films for $x=0.5$. These observations confirmed the high crystalline quality and the epitaxial growth of the YNMO thin films.

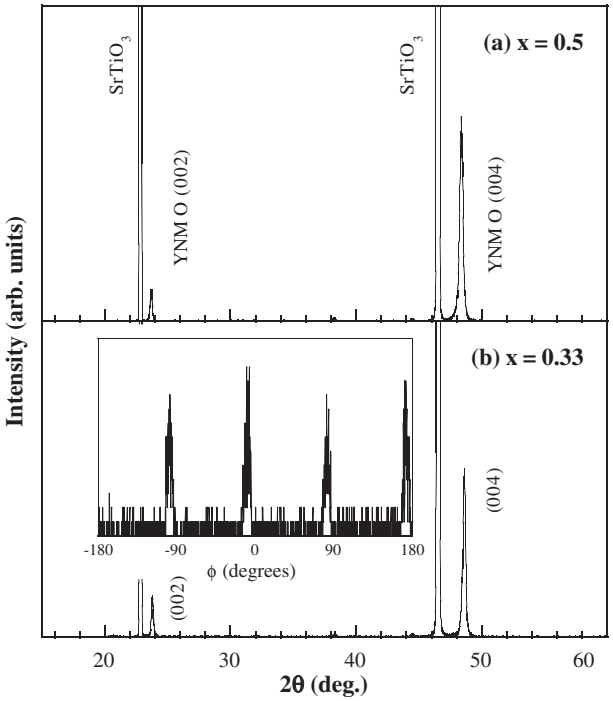

Fig. 1. $\theta-2\theta$ XRD patterns of YNMO films grown on STO substrates for $x=0.33$ and 0.5. Note: two small peaks at $2\theta=38.286°$ and 44.423° were contributed by the sample holder. The inset depicts the φ-scan recorded around the {111}.

Fig. 2 shows the typical SEM images of thin films for $x=0.33$ and 0.5. As we see, the surface of the $x=0.33$ film is covered with spherical grains with an average lateral size of 30 nm. Conversely, for $x=0.5$, the as-grown film consists of in-plane oriented longitudinal islands with an average grain size of 80 nm for the longest distance. In addition, AFM measurements also indicate that the $x=0.5$ film is uniform and dense. The similar result was found for $x=0.33$. Furthermore, there is a decrease in grain size for films grown at low oxygen pressure (for instance, in the case of $x=0.5$, from ~80 nm at 60 Pa to ~30 nm at 25 Pa). Previous studies showed that the magnetic properties of the manganese oxide films are strongly influenced by the morphology. In particular, the ferromagnetic transition temperature T_c degrades as the grain size decreases [8–10]. This is also confirmed by our magnetization results, as shown here below.

In Fig. 3, we show the temperature dependence of the FC and ZFC magnetization at different applied fields for the $x=0.5$ film. As can be seen, the T_c is approximately 85 K compared to that of its bulk at ~80 K. The difference in T_c can be attributed to strain effects induced on the film by the substrate. At low temperatures and low fields, the ZFC magnetization (M) stays more or less constant, then increases rapidly above ~60 K and shows a peak at a temperature (T_f) of ~76 K (also defined as the freezing temperature of clusters [11]). After that, it decreases as in a paramagnetic PM regime.

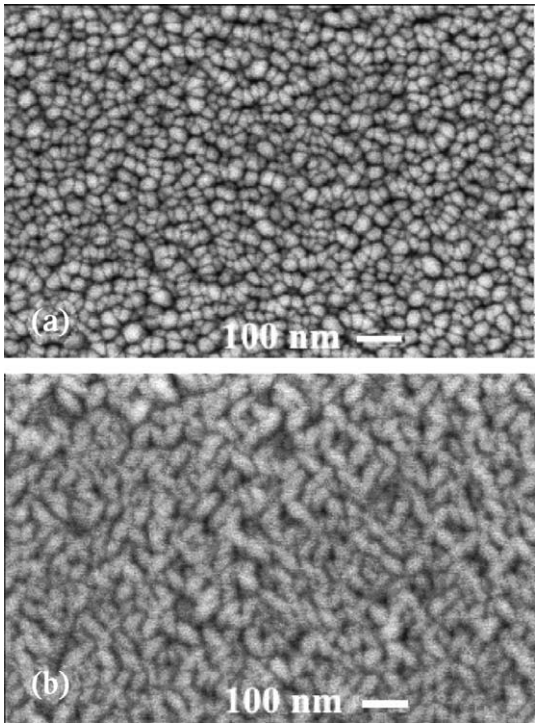

Fig. 2. SEM images of thin films for (a) $x=0.33$ and (b) $x=0.5$.

However, the field-cooled magnetization M_{FC} continuously increases with decreasing temperature. The magnetization has a history dependence with a bifurcation between the ZFC and FC data at an irreversibility temperature T_{irr} (see inset in Fig. 3). At higher fields, T_f and T_{irr} both shift to lower temperature and the $M_{ZFC}(T)$ peak is broadened. There is no difference between M_{ZFC} and M_{FC} in an applied field of 1 T (not shown). This magnetization behavior is quite different from that of bulk samples with same composition, which showed an almost constant magnetization M_{FC} below T_c [6].

The large discrepancy between the FC and ZFC curves is a striking feature implying a rather high coercivity and also suggesting the existence of magnetically ordered small regions

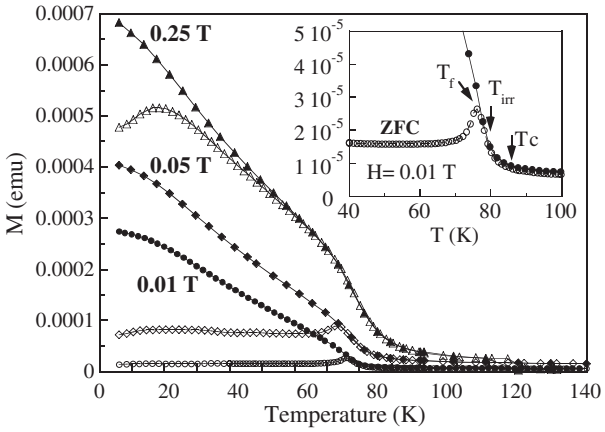

Fig. 3. Field-cooled (closed symbols) and zero-field-cooled (open symbols) magnetization of $x=0.5$ film as a function of temperature, measured at 0.01 (circles), 0.05 (diamonds), and 0.25 T (triangles). Inset shows the enlarged view near the transition temperatures at a field of 0.01 T.

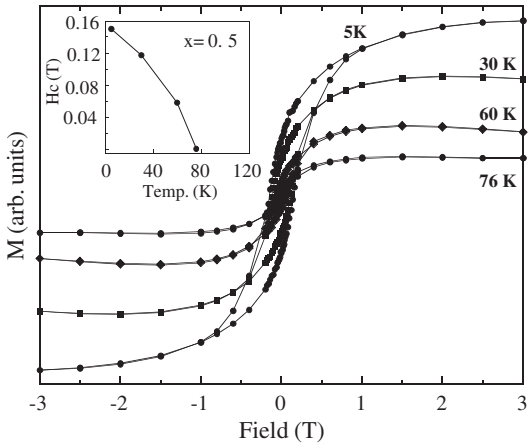

Fig. 4. $M-H$ loops at different temperatures for $x=0.5$. Inset displays temperature variation of the coercivity (H_c) below T_c.

separated by a matrix of disordered spins, which is usually treated as a ‘‘cluster’’ glass state [12,13]. It was claimed that a cluster glass phase has no simple long-range FM order.

In order to understand more deeply the above features of the $M-T$ curves, we investigated the H dependence of M at some typical temperatures for the $x=0.5$ film, as shown in Fig. 4. Clearly, the hysteresis loop at 5 K displays a FM character with a large coercivity of about 0.15 T, much bigger than that of the bulk sample ($H_c=0.02$ T). With increasing temperature, M saturates more easily and the coercivity quickly decreases. At 76 K, where the peak T_f of the ZFC curve locates, the $M-H$ curve shows no hysteresis, but it is nonlinear, indicating a FM behavior. The sharp increase of the coercive field H_c for this sample (see inset in Fig. 4) implies that the film possesses very high magnet–ocrystalline anisotropy. The high value of the anisotropy is then responsible for the low ZFC magnetization values observed for the $x=0.5$ film. In other words, the large values of the coercive field at low temperature further confirm the presence of magnetic clusters, that is, clusters randomly frozen in locally canted states at low temperatures, for which the random anisotropy energy will act as pinning potential [13].

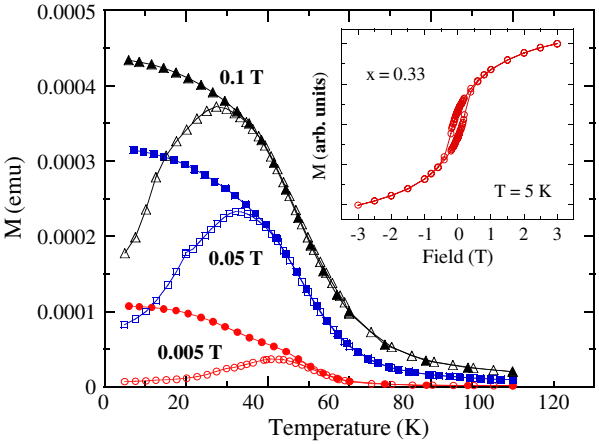

Fig. 5. Field-cooled (closed symbols) and zero-field-cooled (open symbols) magnetization of $x=0.33$ film as a function of temperature, measured at 0.005 (circles), 0.05 (squares), and 0.1 T (triangles). Inset shows $M-H$ loop at 5 K for $x=0.33$.

This also explains the relative difficulty to reach saturation during the $M-H$ lops at 5 K. The same behavior has been found in other materials, e.g. $SrRuO_3$, $La_{0.5}Sr_{0.5}CoO_3$, which are also reported as cluster glass systems [14].

We also studied the magnetic properties of $x=0.33$ films. Fig. 5 displays the $M-T$ curves under ZFC and FC conditions with different applied fields. It is clear that the magnetic behavior of the film is absolutely different from that of the $x=0.5$ film. A clear cusp appears in the ZFC magnetization, indicating that the cluster glass ($x=0.5$) is mostly changed into the spin glass state ($x=0.33$). Note that the $x=0.33$ sample has T_c (60 K) much higher than the reported bulk value (50 K). Furthermore, the $x=0.33$ film shows a spin canting-like transition around 40 K, getting broader and moving downwards in temperature with increasing field, very similar to that of the bulk samples of the same composition [6]. This behavior is believed to be characteristic of canted-antiferromagnetism, in which a ferromagnetic component coexists with predominant antiferromagnetic interactions [13]. $M-H$ measurements confirmed this point, as shown in the inset in Fig. 5: after a steep rise in the low field range, the magnetization at 5 K still increases steadily with increasing magnetic field and does not show any sign of saturation. This is because by increasing the applied field, the ferromagnetic part tends to saturate, whereas the antiferromagnetic part increases linearly, resulting in lack of saturation of magnetization.

From the data mentioned above, there is a clear difference in the ZFC behavior for the $x=0.33$ and $x=0.5$ compositions: while in the former, a pronounced cusp is observed at low and intermediate fields (Fig. 5), in the latter, the M_{ZFC} magnetization shows a constant value at low temperatures (Fig. 3), typically of ferromagnetic domains (or magnetically ordered small regions, i.e., clusters). In the thin films, ferromagnetic coercitivity differs with respect to the one found in bulk materials, since much larger coercive fields are found in thin films of $x=0.5$ composition, due to the anisotropy energy coming from the clusters glass regions randomly frozen at low temperatures. The appearance of cluster glass, indicative of a magnetic disorder, is the evidence for weakening of the DE interaction caused by the structural distortion due to lattice mismatch between the YNMO film and the substrate.

In addition, one can note that a.c. susceptibility would allow to identify more clearly the spin-glass or cluster glasslike behavior, if performed as a function of frequency. However, the very small amount of material deposited as thin film, it becomes hardly possible to get a good signal using this technique.

Since the preparation of manganites with high Mn valency usually requires a post-annealing treatment, we, therefore, investigated the effects of post-deposition thermal processing on T_c and on the microstructure in these two systems. We annealed YNMO films in oxygen atmosphere at 850 °C for 10 h. As shown in Fig. 6, we observed a remarkable improvement in T_c connected to the better crystallinity of the $x=0.33$ film. Indeed, after annealing, the transition temperature T_c is increased from about 60 to 70 K; at the same time, the rocking curve FWHM decreased greatly from 1.02° to 0.3°, illustrating the improvement of the crystalline quality. In

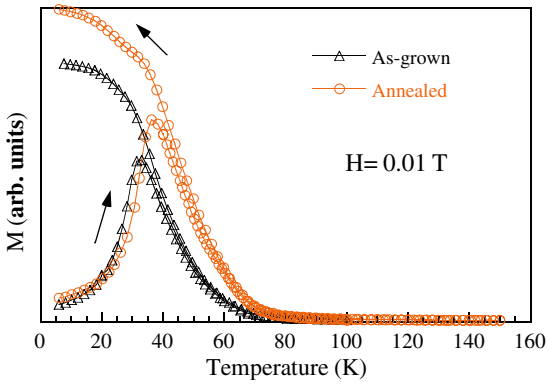

Fig. 6. Temperature dependence of ZFC and FC magnetization for as-grown and annealed (850 °C, 10 h, oxygen atmosphere) YNMO films with x=0.33.

contrast, we found that further annealings have very little effect on the T_c of as-grown films of $x=0.5$ (not shown). Furthermore, XRD characterization showed that there was almost no change in the crystalline mosaicity for this later film. This can be understood in terms of charge–conservation arguments. Annealing under oxygen can usually lead to the increase of the oxygen content of the films and achieve optimum quantity of $Mn^{3+}-Mn^{4+}$ pairs [15–17]. This effect is more pronounced in the case of $x=0.33$. However, in the case of $x=0.5$, almost all manganese is 4+ and the variation in the number of pairs is not so important [5,6]. This indicates that the T_c of the as-grown film for $x=0.5$ is stable, and may be close to its intrinsic maximum value. The details of our studies on the annealing effects will be published elsewhere [18].

4. Conclusions

In summary, we have investigated the structural and magnetic properties of $YNi_xMn_{1-x}O_3$ films deposited on (100) $SrTiO_3$ substrates. We found that the films are single phase and epitaxially grown along the (00l) orientation. The magnetic transition temperatures (T_c) of the films (both $x=0.33$ and 0.5) are higher than the values of the corresponding bulk samples. However, when $x=0.5$, the films show magnetic properties quite different from those of bulk samples. This difference may be caused by the structure distortion in these films.

Acknowledgments

Y. M. thanks Dr. M. Bahout for useful discussions and T. Guizouarn for technical assistance during measurements. Financial support from Region Bretagne is greatly acknowledged. SEM observations were performed at CMEBA at Université de Rennes 1.

References

[1] R. von Helmolt, J. Wecker, B. Holzapfel, L. Schultz, K. Samwer, Phys. Rev. Lett. 71 (1993) 233.
[2] S. Jin, H.M. O'Bryan, T.H. Tiefel, M. McCormack, W.W. Rhodes, Appl. Phys. Lett. 66 (1995) 382.
[3] C. Zener, Phys. Rev 82 (1951) 403.

[4] A.J. Millis, P.B. Littlewood, B.I. Shraiman, Phys. Rev. Lett. 74 (1995) 5144.
[5] C. Moure, D. Gutierrez, O. Pena, P. Duran, J. Solid State Chem. 163 (2002) 377.
[6] O. Peña, M. Bahout, D. Gutierrez, J.F. Fernandez, P. Duran, C. Moure, J. Phys. Chem. Solids 61 (2000) 2019.
[7] Y.W. Ma, M. Guilloux-Viry, P. Barahona, O. Peña, C. Moure, Appl. Phys. Lett. 86 (2005) 062506.
[8] R. Mahesh, R. Mahendiran, A.K. Raychaudhuri, C.N.R. Rao, Appl. Phys. Lett. 68 (1996) 2291.
[9] A. de Andres, J. Rubio, G. Castro, S. Taboada, J.L. Martinez, J.M. Colino, Appl. Phys. Lett. 83 (2003) 713.
[10] A. Haghiri-Gosnet, J. Wolfman, B. Mercey, C. Simon, P. Lecoeur, M. Korzenski, M. Hervieu, R. Desfeux, G. Baldinozzi, J. Appl. Phys. 88 (2000) 4257.
[11] M.A. Señarís-Rodríguez, J.B. Goodenough, J. Solid State Chem. 118 (1995) 323.
[12] M. Ito, I. Natori, S. Kubota, K. Motoya, J. Phys. Soc. Jpn. 63 (1994) 1486.
[13] J.A. Mydosh, Spin Glass: An Experimental Introduction, Taylor and Francis, London, 1993.
[14] P.S.A. Kumar, P.A. Joy, S.K. Date, J. Phys., Condens. Matter 10 (1998) L487.
[15] A. Goyal, M. Rajeswari, R. Shreekala, S.E. Lofland, S.M. Bhagat, T. Boettcher, C. Kwon, R. Ramesh, T. Venkatesan, Appl. Phys. Lett. 71 (1997) 2535.
[16] W. Prellier, M. Rajeswari, T. Venkatesan, R.L. Greene, Appl. Phys. Lett. 75 (1999) 1446.
[17] K.A. Thomas, P.S. de Silva, L.F. Cohen, A. Hossain, M. Rajeswari, T. Venkatesan, R. Hiskes, J.L. MacManus-Driscoll, J. Appl. Phys. 84 (1998) 3939.
[18] Y.W. Ma, M. Guilloux-Viry, P. Barahona, O. Peña, C. Moure, J. Eur. Ceram. Soc. 25 (2005) 2147.